ACS Photonics

Letter

Cite This: ACS Photonics 2018, 5, 353−358

Whisper Gallery Modes in Monolayer Tungsten Disulfide-Hexagonal Boron Nitride Optical Cavity

Tianhua Ren, Peng Song, Jianyi Chen, and Kian Ping Loh*

Department of Chemistry and Centre for Advanced 2D Materials, National University of Singapore, 3 Science Drive 3, Singapore 117543

Supporting Information

ABSTRACT: There are strong interests in constructing nanolasers using two-dimensional transition metal dichalcogenides (TMDs) due to their strong light−matter interactions and high optical gain. However, most cavity designs based on transfer of exfoliated TMDs on silicon oxide are not optimized since monolayer emitters are located far from where the photonic mode reaches maximum intensity. By taking advantage of the excellent dielectric properties of hexagonal boron nitride (h-BN), we design a new microdisk optical cavity fabricated from a van der Waals (VdW) stacked h-BN/WS_2/h-BN. The heterostructure is patterned into microdisk cavities characterized by whispering gallery modes (WGMs). The emission intensity of the WS_2 trion is enhanced by 2.9 times that of exciton in the heterostructure, giving rise to whisper gallery modes with resonance intensities that show nonlinear power dependence. A Rayleigh scatterer directs the cavity emission to vertical collection. Such VdW heterostructure provides an atomically smooth interface that is ideal for low loss photon propagation, giving a Q factor of 1200.

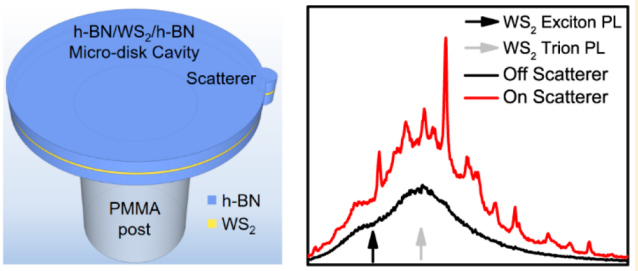

KEYWORDS: *transition metal dichalcogenides, hexagonal boron nitride, optical cavity, whispering gallery mode, trion, heterostructure*

Monolayer transition metal dichalcogenides (TMDs) have attracted interests as a two-dimensional (2D) optical emitterfor nanolasers due to their indirect-to-direct band gap cross-over and strong quantum confinement.[1−4] Lasing operations have been achieved in TMDs by pumping 2D TMDs on optical cavities, such as photonic crystal cavities,[5] microdisk cavities,[6] and nanobeam cavities.[7] Due to their strong exciton emissions, the lasing threshold in monolayer WSe_2 photonic crystal nanolaser has reached as low as 1 W cm^{-2} at cryogenic temperature.[5] Recently, room-temperature lasing has been reported for monolayer $MoTe_2$ in high quality factor (Q) nanobeam cavity.[7] In the demonstrations of laser fabrication, monolayer TMDs were often transferred onto the surface of an empty optical cavity. This cavity design is not optimized for strong light−matter interaction, since monolayer emitters are located far from where photonic mode reaches maximum intensity.[6] Moreover, the TMD transfer process introduces particles and air bubbles into the optical cavity, especially in wet transfer, which brings scattering loss and lower the Q factor.[5,8] Therefore, practical challenges exist for the embedding of 2D monolayer in the core of optical cavity with ultrasmooth interfaces.

To explore various solutions to these problems, here, we design a new microdisk optical cavity directly fabricated from a van der Waals (VdW) heterostructure with monolayer TMDs. We choose WS_2 as the optical emitter due to its higher quantum yield than other TMDs such as MoS_2 and WSe_2.[6] The VdW heterostructure consists of WS_2 sandwiched by two membranes of h-BN, forming a hybrid optical emitter. By controlling the thicknesses of top and bottom h-BN membranes to be equal, the WS_2 can be integrated in the center of heterostructure, where the photonic mode reaches highest electric field. The VdW heterostructure provides an atomically smooth layer-to-layer interface which is ideal for low loss photon propagation. Furthermore, it is discovered that h-BN is an excellent dielectric material for photon confinement, with refractive index as high as 2.3. The heterostructure is further patterned into microdisk cavities with whispering gallery modes (WGMs). By optimizing the WGMs in trion-cavity interaction, a Q factor of 1200 can be achieved.

The monolayer WS_2 and h-BN in VdW heterostructure are mechanically exfoliated, and identified under microscope. As illustrated in Figure 1a, a monolayer WSe_2 and a bulk h-BN (160 nm) flakes were sequentially dry-transferred onto another bulk h-BN (170 nm) on an oxidized silicon substrate. In the transfer protocol, steps 1−3 follow the conventional dry-transfer method.[9] However, to transfer a top layer of h-BN membrane onto the WS_2/h-BN substrate to complete the construction of our optical cavity requires a modification of steps 5 and 6 due to the trapping of air gap (shown in Figure S1(a)); this arises because h-BN/PMMA membrane (total thickness > 360 nm) is stiff and cannot attach conformally onto the bottom surface. If stacks containing air gap are baked, it will

Received: October 21, 2017
Published: November 22, 2017

DOI: 10.1021/acsphotonics.7b01245
ACS Photonics 2018, 5, 353−358

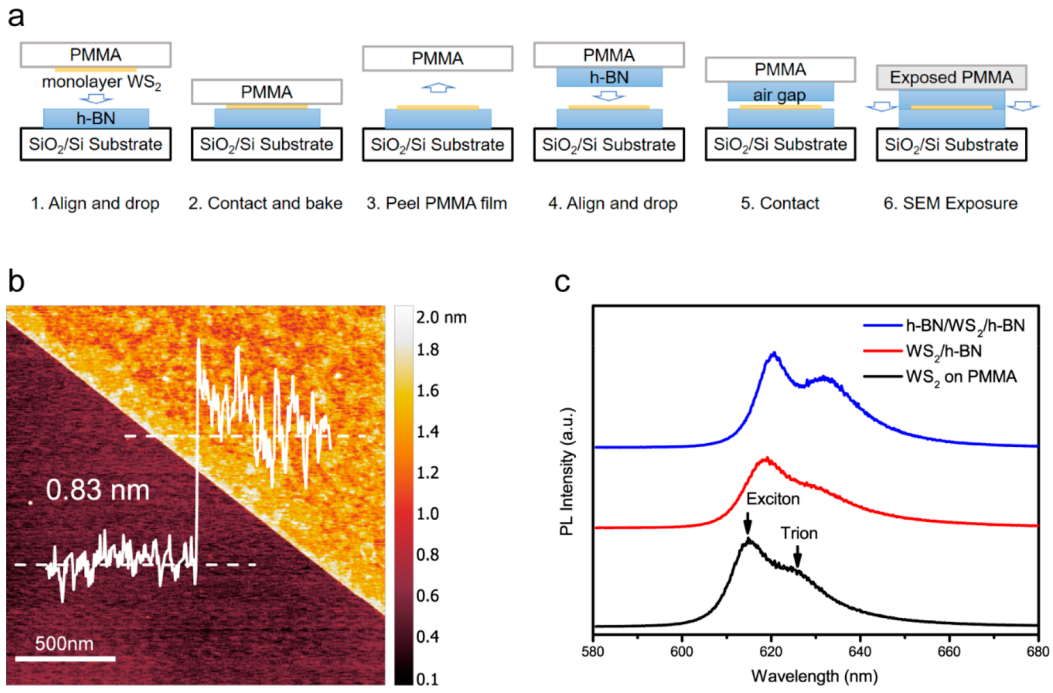

Figure 1. (a) Schematics showing the dry transfer process for the fabrication of the h-BN/WS_2/h-BN heterostructure. (b) AFM topographic image of WS_2/h-BN heterostructure. Line profile showing WS_2 thickness. (c) PL spectra of WS_2 before and after forming heterostructures.

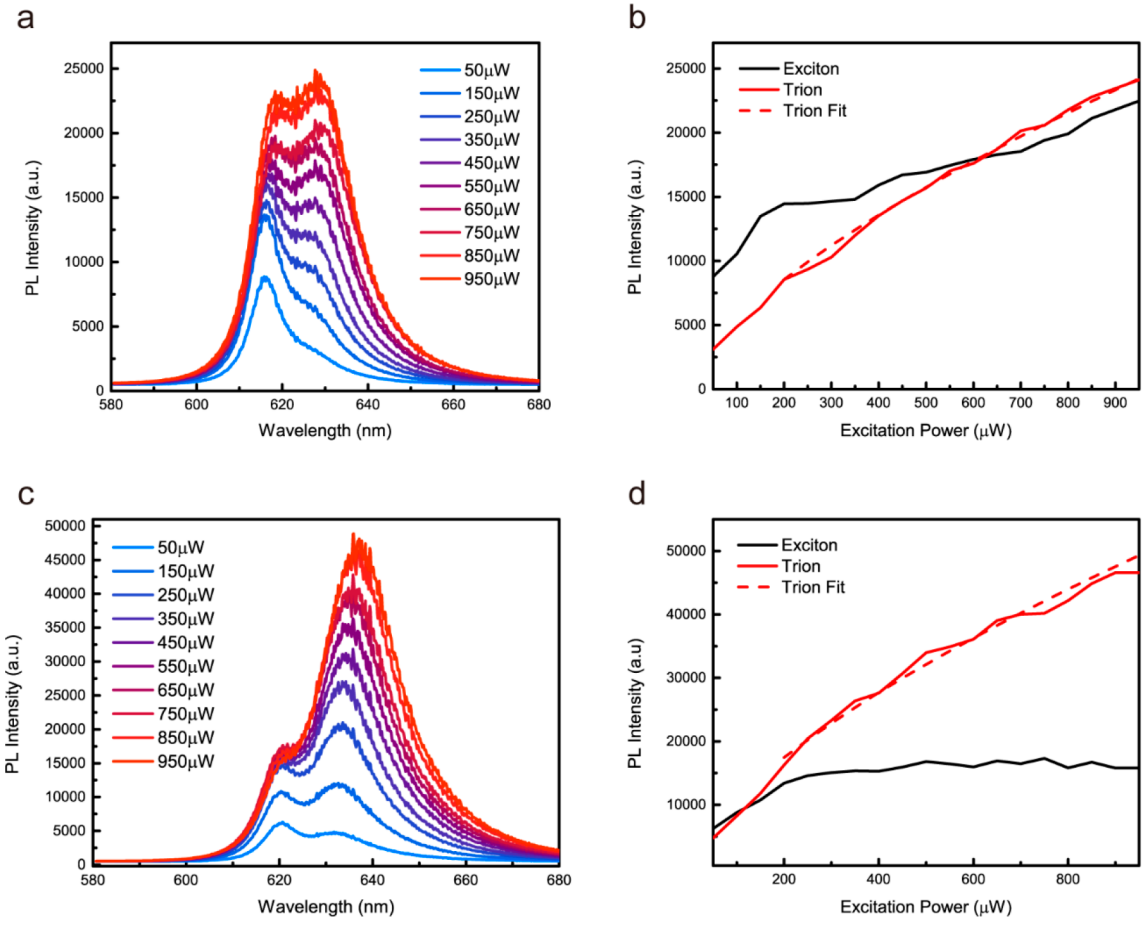

Figure 2. (a) Power-dependent PL for WS_2 on PMMA with (b) the 2/3 power fit for trion PL as a function of laser excitation power. (c) Power-dependent PL for h-BN/WS_2/h-BN, with (d) the 2/3 power fit for trion power-dependent PL.

DOI: 10.1021/acsphotonics.7b01245
ACS Photonics 2018, 5, 353−358

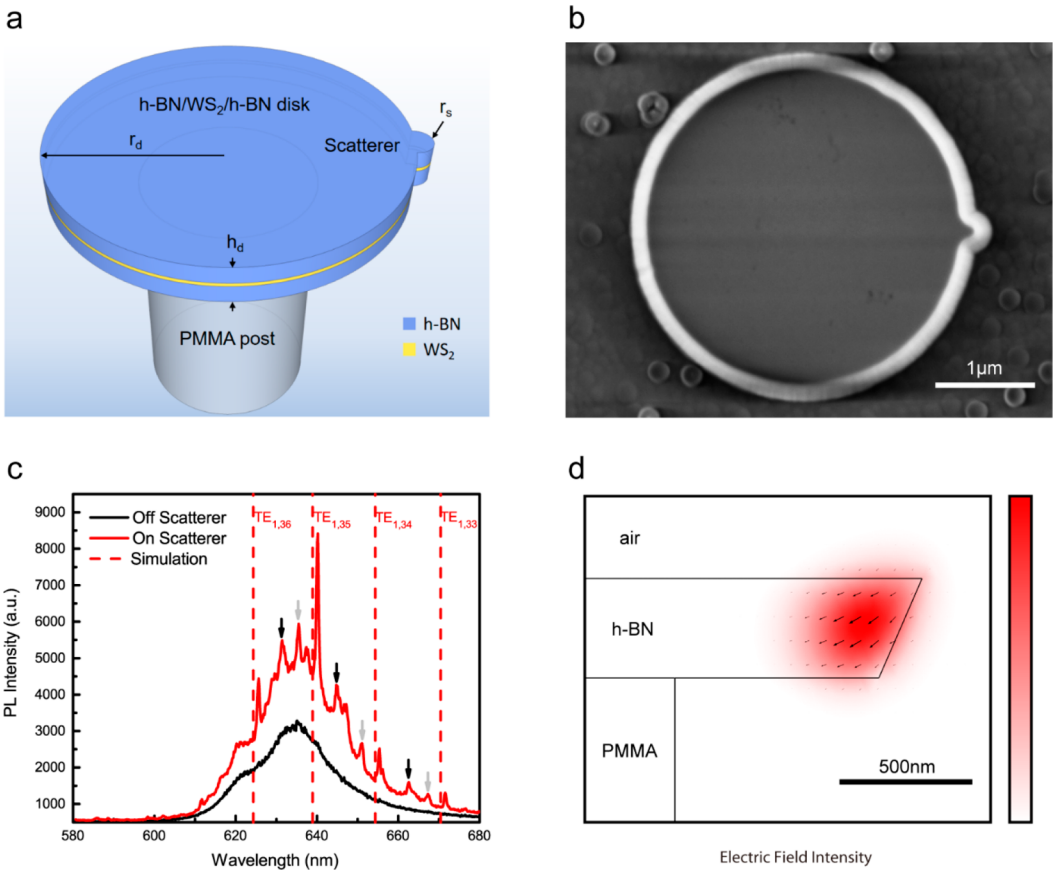

Figure 3. (a) Schematics of microdisk cavity. The cavity consists of a microdisk with radius of r_d and height of h_d, supported by a PMMA post. The disk-shaped scatterer with radius of r_s locates at the edge of microdisk. (b) SEM image of microdisk cavity before transferred onto a PMMA post. (c) PL spectra for r_d = 2 μm and h_d = 330 nm microdisk cavity, with r_s = 0.2 μm nanodisk scatterer. The dashed lines indicated the simulated wavelengths of first order TE modes. $TE_{1,33}$ to $TE_{1,35}$ are coupling with trion, while $TE_{1,36}$ with exciton. Black and gray arrows indicate the second and third order TE modes. (d) Simulated electric field distributions in a cavity cross-section. The red color indicates the electric field intensity of the $TE_{1,35}$ mode, with arrows as the electric field vector.

result in a nonuniform interface. To solve this problem, in step 6, the unbaked PMMA film is electron irradiated in a scanning electron microscopy (SEM) instrument to destroy the cross-links. As a result, the exposed PMMA film becomes softer and thereby allows the top h-BN to contact the substrate conformally without forming air bubble (shown in Figure S1(b)). Finally, the exposed PMMA film can be removed by a standard electron-beam lithography (EBL) development process. Since the dry transfer process avoids the use of wet solvents, the heterostructure interlayer contained minimum contamination.

AFM topographic image in Figure 1b shows that the monolayer WS_2 has a thickness of 0.83 nm with a root mean squared (RMS) roughness of 0.19 nm. The atomically smooth interface of VdW heterostructure provides nearly no optical scattering for high Q optical cavity. The top and bottom h-BN have similar thicknesses, so the WS_2 monolayer can be located at the field maximum of the photonic mode.

At different stages of transfer, photoluminescence (PL) was obtained for the WS_2 pumped by 50 μW (13 kW cm^{-2}) continuous-wave laser in room temperature, as shown in Figure 1c. For WS_2 on PMMA, two broad emission peaks are observed: a high intensity PL peak at 615 nm due to the neutral exciton, and a low intensity peak at 624 nm assigned to the negatively charged exciton (trion).[10] The trion comes from self-doping of the crystal from sulfur vacancy. The WS_2 PL peaks are red-shifted by 4 nm after it is transferred on the surface of h-BN. The redshift in PL spectra suggests that WS_2 bandgap is reduced on h-BN, so quantum confinement for exciton is less on h-BN than on PMMA. When WS_2 is encapsulated by h-BN on either side, the PL intensity of trion increases to the same level as that of the neutral exciton. This behavior, which was also observed for WS_2 in vacuum,[11] suggests that exposure in air suppresses trion emission. This is possibly due to the p-doping by oxygen/water species, which removes electrons necessary for trion formation.[12,13]

Since the trion has strong PL in VdW heterostructure, its absorption effect must be considered in cavity design. If the exciton emission is localized as photonic modes in the optical cavity, there will be trion reabsorption of the photonic modes on the shorter wavelength side near to exciton PL peak, which will decrease the Q factor. Therefore, we design the optical cavity based on resonances with the trion emission, instead of the exciton.

In order to study optical resonances at the trion peak energy, we have to enhance the trion emission relative to the exciton emission. We took advantage of the fact that the relative intensity of the exciton and trion PL could be tuned by varying the excitation power (Figure 2).[10,11] With increasing excitation power, the trion intensity is observed to increase for both WS_2 on PMMA and heterostructure. The power-dependent PL intensity can be fitted by a power function with power of 2/3,

DOI: 10.1021/acsphotonics.7b01245
ACS Photonics 2018, 5, 353−358

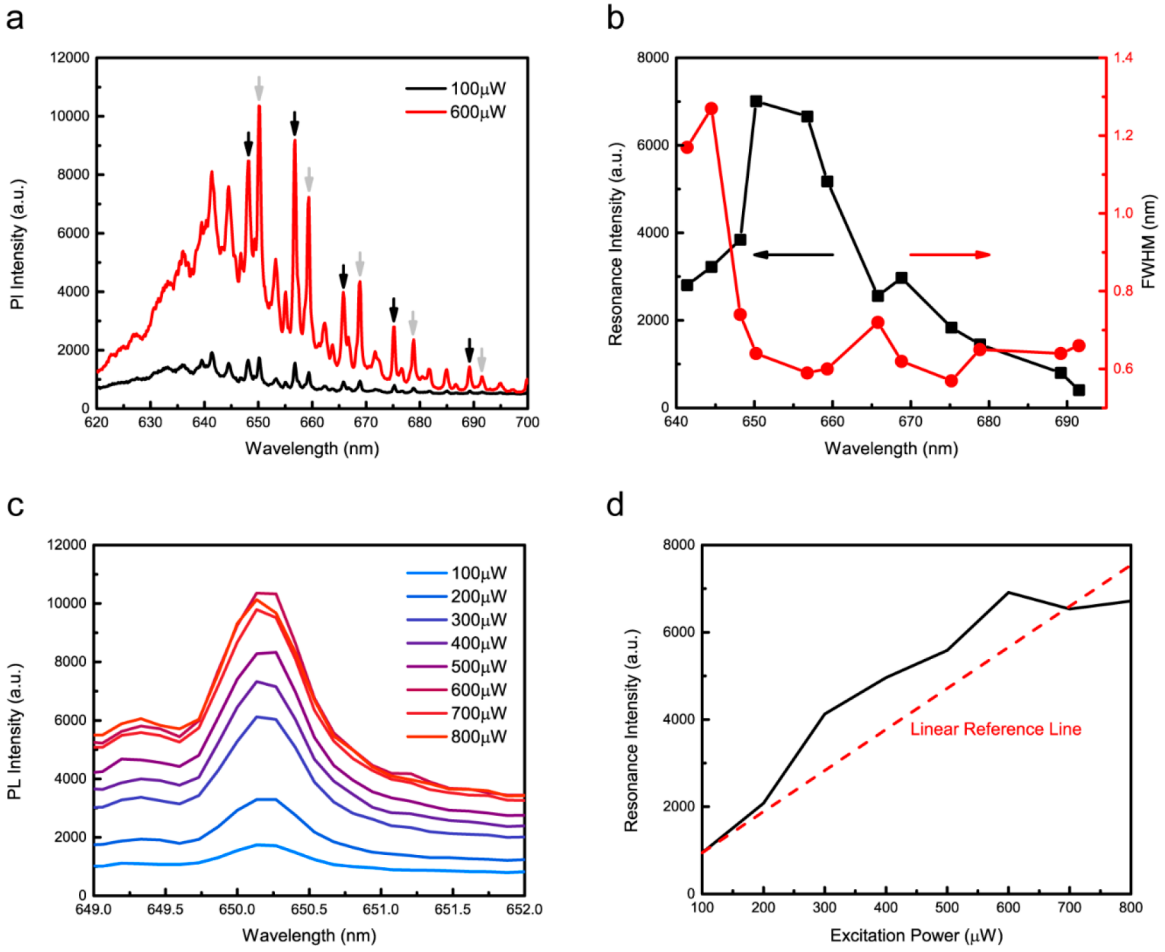

Figure 4. (a) TE_1 resonance peaks within trion PL for the microdisk cavity with r_d = 3.5 μm, h_d = 330 nm, and r_s = 0.35 μm. These PL spectra are tested under different laser pump powers. The high and low frequency branches of a split TE_1 modes are denoted with gray and black arrows, respectively. (b) Resonance peak intensities and width for TE_1 modes at 600 μW (156 kW cm^{-1}) laser excitation power. (c) The power-dependent resonance spectra and (d) intensities for TE_1 at 650 nm wavelength.

confirming this PL peak is from trion emission. For WS_2, exciton intensity is suppressed, so the power-dependent curve is sublinear. The h-BN/WS_2/h-BN heterostructure has its exciton intensity largely suppressed, resulting a trion-to-exciton ratio of 2.9, which is 3 times the ratio in WS_2 on PMMA. As excitation power is increased to 1 mW (260 kW cm^{-2}), the damage threshold of WS_2 is reached, so trion intensity starts to drop with increasing excitation power. Monolayer WS_2 has exciton quantum yield of 0.3% at room temperature.[6] Based on PL intensities obtained from the h-BN/WS_2/h-BN microdisk cavity, the trion quantum yields pumped at 50, 250, and 950 μW are 0.16%, 0.15%, and 0.09%, respectively.

The optical confinement is realized in h-BN/WS_2/h-BN heterostructure by patterning the heterostructure into a microdisk with EBL and reactive ion etcher (RIE). The fabrication of optical cavity is completed by transferring the cavity onto 800 nm thick PMMA film, which is further undercut into a pillar by EBL and development. The PMMA post has a radius $r_{post} = r_d - 1$ μm, allowing the WGM region at disk edge suspended in air. However, this microdisk cavity cannot provide cavity emission in vertical direction for confocal PL detection, because the atomically smooth surface of VdW heterostructure produces little optical scattering from surface.[14] Angle-resolved PL shows that cavity emission is along the in-plane direction (see Figure S3). In order to guide cavity emission in the vertical direction, a Rayleigh scatterer is designed as a nanodisk centered at the edge of microdisk cavity, as illustrated in Figure 3a. When WGMs pass by the scatterer on disk edge, guided photons will be converted to lossy emission in the omni-direction.

SEM image was obtained for the heterostructure cavity on silicon oxide/silicon substrate before transferring it onto the PMMA post, because SEM exposure can damage the PMMA. As shown in Figure 3b, a cavity with r_d = 2 μm, r_s = 0.2 μm, and h_d = 330 nm is achieved with high smoothness and circularity. There are a few defects on the surface of h-BN, which is designed away from the WGM region. In SEM image, the bright ring is the slope surface of disk sidewall. The disk is under-etched during RIE process with top plane radius reduced by 175 nm. Besides, the sidewall is etched with a smooth slope surface by a slow RIE rate of 10 nm/min. The scatterer is also under-etched with its size reduced to about 100 nm. Additionally, the etch residues around the cavity is removed by subsequent transfer process.

The micro-PL is tested with 532 nm excitation laser pumped at 50 μW in room temperature. PL spectra of optical cavity with r_d = 2 μm and r_s = 0.2 μm are shown in Figure 3c. At the scatterer, the resonance peaks appear on PL spectra, while away from the scatterer only the broadband PL peak of WS_2 is observed. As mentioned before, the VdW heterostructure

DOI: 10.1021/acsphotonics.7b01245
ACS Photonics 2018, 5, 353−358

microdisk cannot produce cavity emission in the out-of-plane direction due to the atomically smooth surface, our strategy therefore is to introduce a nanoscatterer cavity, which successfully allows cavity emission to be collected in the out-of-plane direction.

The resonance modes are identified by theoretical analysis. For simplicity, h-BN is assumed to be isotropic dielectric material with index of $n_{\text{h-BN}}$. The $n_{\text{h-BN}}$ is estimated through the WGMs effective refractive index n_{eff}:

$$n_{\text{eff}} = \bar{\lambda}^2/2\pi\bar{R}\Delta\lambda \quad (1)$$

where $\bar{\lambda}$ is the average wavelength of two adjacent m and $m + 1$ WGMs: $\bar{\lambda} = (\lambda_m + \lambda_{m+1})/2$, and m is the WGMs azimuthal number. $\bar{R}$ is the equivalent radius of microdisk, which can be estimated as $\bar{R} = R - d_{\text{edge}}/2$, and d_{edge} is the width of disk slope edge. $\Delta\lambda$ is the mode spacing. In the cavity spectra in Figure 3c, n_{eff} is calculated as 2.31 for two high Q modes around 640 and 655 nm.

The WGMs in microdisk cavities are simulated in COMSOL Multiphysics with 2D axisymmetric method (details in Supporting Information). 2D axisymmetric method is a quasi-3D simulation, but only calculates one cross section of an axisymmetric object with a certain azimuthal number. To simplify the simulation model, WS_2 monolayer is not included in microdisk. The geometry parameters are obtained from SEM and AFM, and the $n_{\text{h-BN}}$ is initialized by using $n_{\text{eff}} = 2.31$. The results provide the wavelengths, the azimuthal number m, and electric field distribution of first order TE modes (TE_1). The $n_{\text{h-BN}}$ is further corrected by fitting simulated $\Delta\lambda$ in PL spectra to arrive at a value of 2.30, indicating that h-BN is a high refractive index material suitable for optical confinement. Using the corrected $n_{\text{h-BN}}$ value, the TE and TM wavelengths are obtained in 2D axisymmetric simulation, with $TE_{1,m}$ modes labeled with azimuthal number m in Figure 3c. The simulated wavelengths are 1 nm away from the measured wavelengths, because the presence of nanoscatterer redshifts the resonance by 1 nm. Since only TE modes are identified in the spectra, the obtained $n_{\text{h-BN}}$ value is the in-plane component $n_{\text{h-BN},\parallel}$, but out-of-plane component $n_{\text{h-BN},\perp}$ remains unknown.

In Figure 3c, the resonance peaks with high Q factor are TE_1 modes, while other low Q modes are second and third order TE modes. TM modes are not clearly identified in this cavity, because monolayer WS_2 couples weakly to out-of-plane polarization. $TE_{1,35}$ mode has a Q factor of $Q = \lambda/\Delta\lambda = 1200$. Considering the scatterer introduces optical loss, it can be inferred that the VdW heterostructure cavity without scatterer should have a higher Q factor. $TE_{1,35}$ is closer to trion central wavelength and receives stronger trion-cavity interaction than adjacent $TE_{1,34}$, so its peak intensity is 4 times stronger than that of $TE_{1,34}$. $TE_{1,33}$ to $TE_{1,35}$ are WGMs which have coupled with trion of WS_2, while $TE_{1,36}$ couples with its exciton. On the shorter wavelength side of PL, due to photon reabsorption in WS_2, the resonance intensities are decreased.

To investigate the trion-cavity interaction, a larger sized microdisk cavity is tested for the resonance peak intensities. In this cavity, which has a larger radius of 3.5 μm, six sets of TE_1 modes appear within the trion broad band emission in Figure 4a. The scatterer splits the TE_1 into two sub modes: high (TE_{1H}) and low (TE_{1L}) frequency modes. The TE_1 peak intensities are plotted in Figure 4b with excitation power of 600 μW (156 kW cm^{-1}). When TE_1 reaches the center wavelength of trion PL, the peak intensities are sharply enhanced, reaching the maximum for TE_{1L} at 650 nm. The full-width-at-half maximums (fwhm) of all TE_1 peaks are ~0.6 nm, except for the reabsorbed modes below 650 nm, indicating that the Rayleigh scatterer limits the TE_1 Q factors to 1100 on average. Furthermore, TE_{1L} at 650 nm is selected to show power-dependent PL in Figure 4c,d. As pump power increases from 100 to 800 μW, the peak intensity rises nonlinearly with excitation power, following the unique power dependence of the trion emission. For pump power from 100 to 600 μW, the resonance intensities exceed the linear relationship by up to 30%. When pump power exceeds 700 μW (182 kW cm^{-1}), the cavity reaches thermal threshold and intensity decreases.

In conclusion, a microdisk optical cavity constructed from h-BN/monolayer-WS_2/h-BN heterostructure was optimized for trion-cavity interaction, generating a 2D trion light source with a Q factor of 1200, and a cavity resonance intensity that showed nonlinear power dependence. Although the nanodisk scatterer helps to collect cavity emission on the atomically smooth cavity surface, it also limits the Q factor. To improve the Q factor to a level necessary for achieving lasing at room temperature, one strategy is to use a tapered optical fiber to collect the cavity emission. This work also highlights that h-BN is an excellent dielectric material for optical modes confinement, thus h-BN heterostructures should be deployable in on-chip optical waveguides and cavities.

METHOD

To fabricate the VdW heterostructure, monolayer WSe_2 and h-BN (crystals from HQ graphene) were mechanically exfoliated on 200 nm PMMA (MicroChem 495A4) coated silicon substrate or oxidized silicon substrate. SEM (FEI Verios460 FESEM) exposure is conducted for top h-BN transfer with 100 pA and 20 kV. The flakes were annealed at 120 °C after steps 3 and 6 in Figure 1a. The VdW heterostructures were further patterned into microdisks by EBL (Jeol EBL 6300FS with 100 pA current) and deep RIE (Oxford Plasma Pro Cobra 100, with 40 W RF power and 40 sccm CHF_3 and 4 sccm O_2). Cavity resonance spectra were measured by commercial confocal photoluminescence microscopy (Alpha 300 R) at room temperature. The 532 nm continuous-wave laser pumped WS_2 in cavities at room temperature, vertically through a 100× objective lens, focusing to a 700 nm diameter spot. The PL was also collected through the same lens to spectrometer.

ASSOCIATED CONTENT

Supporting Information

The Supporting Information is available free of charge on the ACS Publications website at DOI: 10.1021/acsphotonics.7b01245.

Additional information on the transfer methods, AFM of the heterostructures, PL spectra of h-BN, and emission characteristics of the optical microdisk cavity without scatterer (Figures S1−S3; PDF).

AUTHOR INFORMATION

Corresponding Author

*E-mail: chmlohkp@nus.edu.sg.

ORCID

Tianhua Ren: 0000-0002-3647-3219
Jianyi Chen: 0000-0002-3757-7634
Kian Ping Loh: 0000-0002-1491-743X

DOI: 10.1021/acsphotonics.7b01245
ACS Photonics 2018, 5, 353−358

Notes

The authors declare no competing financial interest.

REFERENCES

(1) Mak, K. F.; Lee, C.; Hone, J.; Shan, J.; Heinz, T. F. Atomically Thin MoS_2: A New Direct-Gap Semiconductor. *Phys. Rev. Lett.* **2010**, *105*, 136805.

(2) Splendiani, A.; Sun, L.; Zhang, Y.; Li, T.; Kim, J.; Chim, C. Y.; Galli, G.; Wang, F. Emerging Photoluminescence in Monolayer MoS_2. *Nano Lett.* **2010**, *10*, 1271−1275.

(3) He, K.; Kumar, N.; Zhao, L.; Wang, Z.; Mak, K. F.; Zhao, H.; Shan, J. Tightly Bound Excitons in Monolayer WSe_2. *Phys. Rev. Lett.* **2014**, *113*, 26803.

(4) Chernikov, A.; Berkelbach, T. C.; Hill, H. M.; Rigosi, A.; Li, Y.; Aslan, O. B.; Reichman, D. R.; Hybertsen, M. S.; Heinz, T. F. Exciton Binding Energy and Nonhydrogenic Rydberg Series in Monolayer WS_2. *Phys. Rev. Lett.* **2014**, *113*, 76802.

(5) Wu, S.; Buckley, S.; Schaibley, J. R.; Feng, L.; Yan, J.; Mandrus, D. G.; Hatami, F.; Yao, W.; Vučković, J.; Majumdar, A.; Xu, X. Monolayer Semiconductor Nanocavity Lasers with Ultralow Thresholds. *Nature* **2015**, *520*, 69−72.

(6) Ye, Y.; Wong, Z. J.; Lu, X.; Ni, X.; Zhu, H.; Chen, X.; Wang, Y.; Zhang, X. Monolayer Excitonic Laser. *Nat. Photonics* **2015**, *9*, 733−737.

(7) Li, Y.; Zhang, J.; Huang, D.; Sun, H.; Fan, F.; Feng, J.; Wang, Z.; Ning, C. Z. Room-Temperature Continuous-Wave Lasing from Monolayer Molybdenum Ditelluride Integrated with a Silicon Nanobeam Cavity. *Nat. Nanotechnol.* **2017**, *12*, 987−992.

(8) Majumdar, A. Dielectric Resonator Integrated 2D Material Structures. *Adv. Photonics 2017 (IPR, NOMA, Sensors, Networks, SPPCom, PS)* **2017**, 2−4.

(9) Withers, F.; Del Pozo-Zamudio, O.; Mishchenko, A.; Rooney, A. P.; Gholinia, A.; Watanabe, K.; Taniguchi, T.; Haigh, S. J.; Geim, A. K.; Tartakovskii, A. I.; Novoselov, K. S. Light-Emitting Diodes by Band-Structure Engineering in van Der Waals Heterostructures. *Nat. Mater.* **2015**, *14*, 301−306.

(10) Mitioglu, A. A.; Plochocka, P.; Jadczak, J. N.; Escoffier, W.; Rikken, G. L. J. A.; Kulyuk, L.; Maude, D. K. Optical Manipulation of the Exciton Charge State in Single-Layer Tungsten Disulfide. *Phys. Rev. B: Condens. Matter Mater. Phys.* **2013**, *88*, 245403.

(11) Currie, M.; Hanbicki, A. T.; Kioseoglou, G.; Jonker, B. T. Optical Control of Charged Exciton States in Tungsten Disulfide. *Appl. Phys. Lett.* **2015**, *106*, 201907.

(12) Tongay, S.; Zhou, J.; Ataca, C.; Liu, J.; Kang, J. S.; Matthews, T. S.; You, L.; Li, J.; Grossman, J. C.; Wu, J. Broad-Range Modulation of Light Emission in Two-Dimensional Semiconductors by Molecular Physisorption Gating. *Nano Lett.* **2013**, *13*, 2831−2836.

(13) Peimyoo, N.; Yang, W.; Shang, J.; Shen, X.; Wang, Y.; Yu, T. Chemically Driven Tunable Light Emission of Charged and Neutral Excitons in Monolayer WS_2. *ACS Nano* **2014**, *8*, 11320−11329.

(14) Peter, E.; Dousse, A.; Voisin, P.; Lemàtre, A.; Martrou, D.; Cavanna, A.; Bloch, J.; Senellart, P. Highly Directional Radiation Pattern of Microdisk Cavities. *Appl. Phys. Lett.* **2007**, *91*, 151103.

DOI: 10.1021/acsphotonics.7b01245
ACS Photonics 2018, 5, 353−358